Available online at www.sciencedirect.com
SCIENCE DIRECT®
Journal of Hydrology 317 (2006) 1–16
Journal of Hydrology
www.elsevier.com/locate/jhydrol

Reducing concentration uncertainty using the coupled Markov chain approach

Amro M.M. Elfeki[1,*]

Water Resources Section, Faculty of Civil Engineering and Geosciences, Delft University of Technology
P.O. Box 5048, 2600 GA, Delft, The Netherlands

Received 22 December 2003; revised 14 April 2005; accepted 14 April 2005

Abstract

This paper presents a framework for coupling the stochastic technique that is called 'coupled Markov chain' (Elfeki and Dekking, 2001), which is used for stochastic site characterization, with numerical groundwater flow and transport models. The purpose is to study the reduction of uncertainty on concentration distribution by conditioning on a number of boreholes using the Monte-Carlo approach. This study addresses some issues that have not been given much attention in the literature, namely: (1) using the so-called CMC (Coupled Markov Chain) model for modeling heterogeneity as a non-Gaussian field characterized by multi-dimensional transition probabilities rather than variograms or autocorrelation functions, (2) considering a hydrodynamic flow field that is non-uniform in the mean flow due to boundary conditions where flow is driven from the left top corner moving to the right domain boundary, and (3) utilizing the concept of forward modeling in the framework of conditioning on geological borehole information (geometrical configuration), rather than conditioning on direct measurements of the hydrogeological parameters (e.g. hydraulic conductivity, porosity, etc.).

The model is applied on an unconsolidated deposit located in the central Rhine-Meuse delta in the Netherlands. The data at the site is merely used to calculate the transition probabilities used in the CMC model to generate a reference geological model for the rest of the analysis. The results show the potential applicability of the CMC model in reducing the uncertainty in concentration fields when a sufficient number of boreholes are available. Reproduction of peak concentrations, breakthrough curves and plume spatial moments require many conditioning boreholes (in this case study 25–31 boreholes with 10–8 m spacing over a distance of 240 m). However, reproduction of plume shapes requires a lot less boreholes (in this case study five boreholes with 60 m spacing over a distance of 240 m).

Keywords: Coupled Markov chains; Stochastic modeling; Subsurface heterogeneity; Conditioning; Uncertainty quantification; Flow and transport in porous medium

* Address: Department of Hydrology and Water, Resources Management, King Abdulaziz University, P.O. Box 80208, Jeddah 21589, Saudi Arabia. Fax: +31 15 2785915.
E-mail address: amro_elfeki@yahoo.com.
[1] On leave from Faculty of Engineering, Mansoura University, Mansoura, Egypt.

0022-1694/$ - see front matter © 2005 Elsevier B.V. All rights reserved.
doi:10.1016/j.jhydrol.2005.04.029

1. Introduction

Groundwater contamination became an important environmental issue which poses a serious threat to drinking water quality. The simulation of contaminant transport through the subsurface is necessary in order to effectively design mitigation methods for cleanup and prevention of the deterioration of the subsurface-water. It is well known that natural heterogeneity and the large scale spatial variability of the hydraulic conductivity controls the flow field and hence the spreading of contaminant plumes in the subsurface (see e.g. the Borden landfill in Ont., Canada (Sudicky, 1986), the MADE site at Columbus Air Force Base in Mississippi (Boggs et al., 1992), and Cape Cod, MA, USA (Hess et al., 1992).

Our inability to characterize subsurface heterogeneity properly makes predictions of contaminant concentration highly uncertain. All theories reviewed by Dagan (1989) and Gelhar (1993) describe plumes by means of a few global measures such as the centroid (first moment) of the plume and the spreading around that centroid (second moment). Most of these theories rely on assumptions of global stationarity of the heterogeneous medium and log–normal distribution of the hydraulic conductivity. They are derived in the context of continuum mechanics leading to upscaled transport parameters (e.g. macro-dispersion tensor). However, in subsurface geological formations discrete geometrical structures exist (see e.g. some outcrops, among many others, in the Oude Maas deposit, The Netherlands; Ref. Van Beek and Koster, 1972, and Weber et al., 1972; a palaeo Rhine distributary in the Netherlands). These discrete features render simple concepts of continuum mechanics invalid at field scale. The use of scale averaging on transport of contaminants can lead to unreliable prediction of contaminant spreading (e.g. the existence of high conductivity preferential flow paths and low conductivity barriers are smeared out resulting in non-physical model parameters and predicted plumes that are smoother than observed ones). Therefore, application of the existing theories (based on Guassian random fields) in a highly complex geological setting with discrete features and the existence of preferential flow paths is still questionable.

Maps of heterogeneity must represent features that are consequential to flow and transport processes to minimize the uncertainty of flow and concentration fields. Many studies focused on minimizing concentration uncertainty by conditioning the hydraulic conductivity fields either on measurements of hydraulic conductivity (e.g. using Kriging techniques or Gaussian conditional probability distributions) in solving the forward (direct) groundwater flow and transport problems (e.g. recent work by van Leeuwen (2000)), or by conditioning on groundwater head data and/or concentration data (see e.g. recent work by Valstar (2001) and Bakr et al. (2003) using the method of representer) in solving the inverse groundwater flow and transport problems. The forward modeling approach has the advantage of being well-posed and efficient in terms of computer costs. Elfeki et al. (1998) performed Monte-Carlo numerical simulations in a forward framework to study flow and transport using unconditional coupled Markov chain model for quantification of uncertainty in concentration distributions. They distinguished three different types of uncertainties: geological uncertainty in which the geological configuration of the units is uncertain and characterized by transition probabilities, while the conductivity value in each unit is assumed uniform and known in a deterministic sense. Parametric uncertainty assumes that the geological structure is known deterministically while the parameter value at each unit is subjected to uncertainty characterized by a stationary Gaussian field. This is a plausible geological assumption for some sites, like some outcrops), and both parametric and geological uncertainties where both the geological structure and parameter values are uncertain. The last one is the worst case scenario where information is lacking on both the geological structures and the parameter values of each unit. One of their conclusions emphasized the early work by Smith and Schwartz (1981) where the uncertainty can be strongly reduced when deterministic information is available about the geological structure (e.g. interfaces between geological units).

In this study, the concept of geological uncertainty is adopted. This means that the geological structure is considered uncertain, it is only known through the transition probabilities. However, the K value of each unit is known in a deterministic sense. So, each

generated realization, by the CMC model, in the Monte-Carlo framework produces a realization of the configuration of the geological structure, while the parameter value of each structure is supposed to be known deterministically. This assumption can be justified from the practical point of view where measurements are often lacking about the subsurface parameters. Engineers often use data about hydrological parameters from the literature. However, geological boreholes may provide some data to delineate the geological configuration while in between the boreholes the geological configuration, continuity and discontinuity of the layers are uncertain. Therefore, the conditioning is formulated in a forward modeling framework. However, instead of conditioning on measurements of hydraulic conductivity, the conditioning is performed on the geological structures predicted from borehole data. This research presents a Monte-Carlo framework for coupling the stochastic technique called 'coupled Markov chain' (Elfeki and Dekking, 2001) with numerical groundwater and transport models to predict concentration distribution of contaminant plumes in the subsurface layers with the associated uncertainty in concentration distribution. The goal of this study is to address some aspects that are not given much attention in the literature,

1. using the so-called CMC (Coupled Markov Chain) model for modeling heterogeneity as a non-Gaussian (and non-stationary) field characterized by multi-dimensional transition probabilities rather than variograms or autocorrelation functions,
2. considering the hydrodynamic flow field that is non-uniform in the mean due to boundary conditions where flow is driven from the left top corner moving towards the right domain boundary. Many researches consider a flow field that it is driven from left to right. However, in this study we considered flow, which is non-uniform in the mean at the macroscopic level to simulate seepage form landfill, to deviate from the literature and to explore other hydrodynamic conditions. However, the boundary conditions are fixed head boundaries and assumed certain, and
3. utilizing the concept of forward modeling in the framework of conditioning on geological boreholes information (geometrical configuration) rather than conditioning on direct measurements of the hydrogeological parameters (e.g. hydraulic conductivity, porosity, etc.).

The above mentioned issues have been investigated through the application of the CMC model, flow and transport models on an unconsolidated deposit located in the central Rhine-Meuse delta (the Gorkum study area Fig. 1) in the Netherlands.

2. Cross-section data

The Gorkum study area is located in the central Rhine-Meuse delta in the Netherlands. Fig. 1 shows the geological cross-section, interpreted by geologists based on drillings made at 20 m apart (for details see Weerts and Bierkens, 1993; Bierkens and Weerts, 1994; and Weerts, 1996). Six lithogenetic units are distinguished; channel deposits (sand), natural levee deposits (fine sand, sandy clay, silty clay), crevasse deposits (fine sand, sandy clay, silty clay), flood basin deposits (clay, humic clay), peat and the subsoil that consists of sandy eolian and fluvial sediments. The data at the site is merely used to calculate the transition probabilities used in the CMC model to generate a reference geological model for the rest of the analysis.

3. Description of the coupled Markov chain model

The coupled Markov chain (CMC) model (Elfeki and Dekking, 2001) is applied on the cross-section given in Fig. 1. A brief description of the coupled Markov chain model is given below. The model is stochastic in nature, and couples two Markov chains. The first one is used to describe the sequence of lithologies in the vertical direction, and the second in the horizontal direction. The two chains are coupled in the sense that a state of a cell (i, j) in the domain depends on the state of two cells, the one on top: $(i, j-1)$, and the other on the left: $(i-1, j)$ of the current cell (Fig. 2 top). The model is very general, it can handle any three cells from various directions. We can even have four possibilities namely top and left (as in this case), bottom and left, right and bottom, and right and top. This type of modeling approach is called unilateral Markov random fields (see e.g. Galbraith

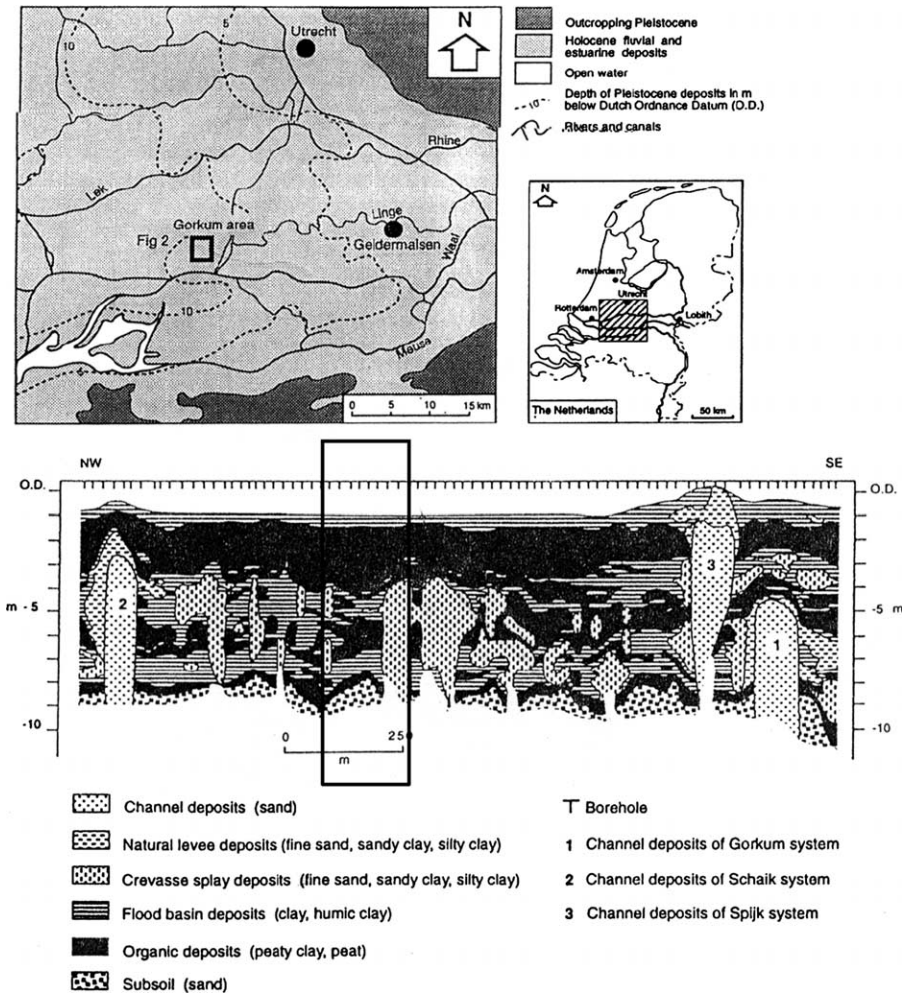

Fig. 1. Map location of the study area and cross-section showing the deposits of the Holocene fluvial systems, Weerts and Bierkens (1993): Top images show the map of the Netherlands and the site location. The bottom image shows the overall cross-section drawn from the boreholes, the window on the image is the part used for transport simulations. Note the vertical exaggeration.

and Walley, 1976). The reason behind this choice is twofold: first is to develop an efficient generation algorithm of Markovian fields. Traditional Markov random fields (Cross and Jain, 1983) use dependence of four neighboring cells that leads to implicit formulation of the generation algorithm. This procedure becomes inefficient in terms of computer time and does not produce satisfactory results from the geological point of view (see Cross and Jain, 1983). Second is that in field situations, data are usually in the form of boreholes (vertical variability) and surface knowledge (horizontal variability) is gained from the geological survey. The technique tries to propagate the knowledge available on the left vertical and top horizontal boundaries through the horizontal and vertical chains, respectively, into the cells inside the domain. The dependence of the cells is described in terms of transition probabilities from the two chains as

$$p_{lm,k} := \Pr(Z_{i,j} = S_k | Z_{i-1,j} = S_l, Z_{i,j-1} = S_m)$$

$$= \frac{p^{\mathrm{h}}_{lk} p^{\mathrm{v}}_{mk}}{\sum_f p^{\mathrm{h}}_{lf} p^{\mathrm{v}}_{mf}} \quad k = 1, \ldots, n \tag{1}$$

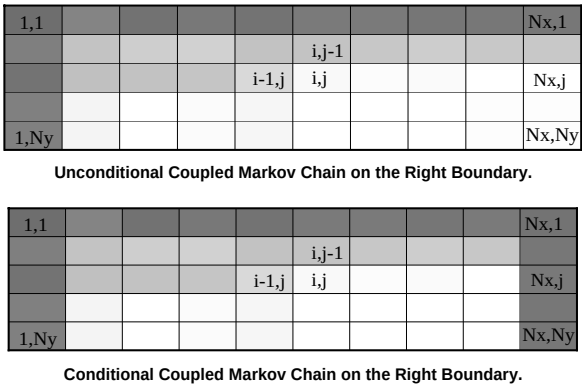

Fig. 2. Numbering system in a two-dimensional domain for the coupled Markov chain model. Unconditional coupled Markov chain (top), and the coupled Markov chain conditioned on future states (bottom). Dark grey cells are known boundary cells, light grey cells are known cells inside the domain (previously generated, the past) white cells are unknown cells. The future state used to determine the state of cell (i, j) is the state on the same level at cell (N_x, j) (from Elfeki and Dekking, 2001).

where $p_{lm,\,k}$ is the probability that cell (i, j) is in state S_k given that cell $(i-1, j)$ is in state S_l and cell $(i, j-1)$ is in state S_m, $Z_{i,\,j}$ is the state of cell (i, j), $Z_{i-1,\,j}$ is the state of cell $(i-1, j)$, $Z_{i,\,j-1}$ is the state of cell $(i-1, j)$, p^{h}_{lk} and p^{v}_{mk} are the corresponding elements of the horizontal (superscript h) and vertical (superscript v) transition probability matrices and n is the number of states in the geological system.

An extension of the coupled Markov chain model to enable conditioning on any number of boreholes is achieved in Elfeki and Dekking (2001). The methodology is based on the concept of conditioning a one-dimensional horizontal Markov chain on future states (Fig. 2 bottom). The conditioning is performed in an explicit way. This makes the methodology efficient in terms of computer time and storage in comparison with other techniques available in the literature (e.g. simulated annealing see Parks et al., 2000). The conditioning formula is given by,

$$\begin{aligned} p_{lm,k|q} &:= \Pr(Z_{i,j} = S_k | Z_{i-1,j} = S_l, Z_{i,j-1} \\ &\quad = S_m, Z_{N_x,j} = S_q) \\ &= \frac{p^{\mathrm{h}}_{lk} p^{\mathrm{h}(N_x-i)}_{kq} p^{\mathrm{v}}_{mk}}{\sum_f p^{\mathrm{h}}_{lf} p^{\mathrm{h}(N_x-i)}_{fq} p^{\mathrm{v}}_{mf}}, \quad k = 1, \ldots, n \end{aligned} \tag{2}$$

where $p_{lm,\,k|q}$ is the probability that cell (i, j) is in state S_k given that cell $(i-1, j)$ is in state S_l and cell $(i, j-1)$ is in state S_m and cell (N_x, j) is in state S_q, and $p^{\mathrm{h}(N_x-i)}_{kq}$ is the probability to go from S_k to S_q in (N_x-i)-steps.

The transition probabilities are obtained by superimposing a grid with equidistant cells ($\Delta x = 2$ m, $\Delta y = 0.25$ m) in both vertical and horizontal directions over the geological map (Fig. 1 the window part). Choosing cell dimensions correspond to some rule of thumb (Lin and Harbaugh, 1984): the minimum sizes of the geological features observed in the cross-section. Smaller cell sizes would lead to higher resolution while more computational efforts are needed. Larger cell sizes would lead to less computational efforts while simmering out some geological features (Lin and Harbaugh, 1984). The transition frequencies (e.g. in the vertical direction) are calculated between the states by counting how many times a given state S_l is followed by itself or by other state S_k in the vertical direction, and then it is divided by the total number of transitions in the vertical direction (Elfeki and Dekking, 2001). Similar procedure is made for the horizontal direction. Table 1 shows the computed statistics from Fig. 1 (the window part).

4. Sensitivity analysis of the model parameters

Bierkens (1996) has performed both laboratory tests and utilization of empirical equations to estimate the hydraulic and geometrical parameters of the samples collected from the site. Some of these parameters are given in Table 2. In the present study, we considered constant porosity, which is set to a value of 0.3. Bierkens (1996)) showed, however, that the porosity values in the Fig. 1 cross-section are not constant. Since, our main interest is to investigate the effect of conditioning on the geometric configuration and consequently on the solute plumes, whatever the model parameters are, we fell that the simplification of a constant porosity is justifiable. For the purpose of transport simulations there was no data available regarding dispersivities. Therefore, the dispersivity is also considered constant, and is set to 0.1 m in the longitudinal direction and to 0.01 m in the vertical one (Fig. 3).

Table 1
Horizontal and vertical transition probability matrices of the 240 m section (modified from Keshta, 2003)

Length of the given section = 240 m
Sampling interval in *X*-direction = 2 m
No. of states = 4
Horizontal transition probability matrix

State	3	4	5	6
3	0.979	0.010	0.011	0.000
4	0.011	0.974	0.015	0.000
5	0.008	0.012	0.977	0.003
6	0.010	0.000	0.007	0.983

Depth of the given section = 10 m
Sampling interval in *Y*-direction = 0.25 m
Vertical transition probability matrix

State	3	4	5	6
3	0.969	0.027	0.004	0.000
4	0.008	0.724	0.268	0.000
5	0.025	0.139	0.791	0.045
6	0.000	0.000	0.000	1.000

Table 2
Soil properties at core scale of the 240 m × 10 m cross-section (Bierkens, 1996)

Code (*i*)	Soil type	W_i	$\langle Y_i \rangle$	$\sigma^2_{Y_i}$	$\langle K_i \rangle$ m/day	$\sigma^2_{K_i}$
3	Sand and silty clay	0.19	−4.97	3.49	0.1	5.86
4	Clay and humic clay	0.30	−7.00	2.49	0.01	10.1
5	Peat	0.39	−2.00	1.7	0.30	2.99
6	Fine and loamy sand	0.12	0.60	1.76	4.40	0.09

W_i, $\langle K_i \rangle$, $\sigma^2_{K_i}$, $\langle Y_i \rangle$, $\sigma^2_{Y_i}$ are the proportion in the cross-section, mean and variance of conductivity, logarithmic transformation of mean and variance of conductivity of lithology (*i*), respectively.

Trial numerical experiments have been performed to study the accuracy of the flow model under the given hydraulic conductivity contrast. The criterion for convergence in the solution of the flow problem is that the sum of residuals should be small enough. Three accuracy limits are tested namely 0.001, 0.0001 and 0.00001. It has been shown that an accuracy limit of 0.0001 is reasonable in terms of stable results and computational costs (Keshta, 2003).

For stability of the Monte-Carlo realizations, 50 and 100 realizations are tested to study the convergence of the computations. Table 3 shows the flow and transport parameters used in the numerical experiments. In the Monte-Carlo runs, the mean concentration fields are constructed by averaging the solute concentrations over the total number of realizations. Ensemble average concentrations $\langle C(\mathbf{x}, t) \rangle$ can be determined at each grid point as

$$\langle C(\mathbf{x}, t) \rangle = \frac{1}{\mathrm{MC}} \sum_{k=1}^{\mathrm{MC}} C_k(\mathbf{x}, t), \tag{3}$$

$C_k(\mathbf{x}, t)$ is the concentration at a given t, and location $\mathbf{x}$ in the kth realization.

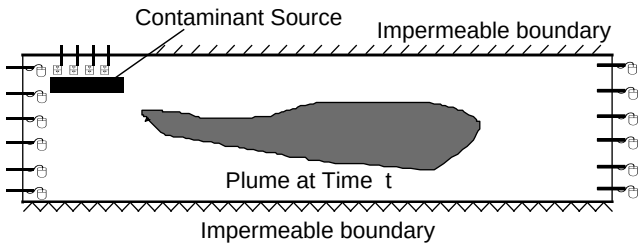

Fig. 3. Schematic representation of the flow and transport problems in this study.

Table 3
Numerical simulation values used in the numerical tracer experiment

Parameter	Numerical value
Domain dimensions	$L_x=240$ m, $L_y=10$ m
Domain discretization	$\Delta x=2$ m, $\Delta y=0.25$ m
Average head difference over the domain	1.0 m
Injected tracer mass	1000 g
Number of particles	10,000 Particles
Time step in calculations	5 days
Longitudinal pore-scale dispersivity	0.10 m
Transverse pore-scale dispersivity	0.01 m
Effective porosity	0.30
X- and Y-coordinates of injection source	15 m, −2.0 m
Initial source dimensions	Width = 20.0 m and Depth = 1.0 m
Retardation coefficient	1.0
Diffusion coefficient	0.0

This ensemble average $\langle C(\mathbf{x}, t)\rangle$ can be interpreted as the imaginary envelope of the performance determined by all possible realizations (Fischer et al., 1979). For a real field situation, however, there is always a single (actual) realization. Therefore, one could expect to find the actual plume within the imaginary envelope given by the expected value of the concentration field. The concentration variance at each grid point is given by

$$\sigma_C^2(\mathbf{x},t)=\frac{1}{\mathrm{MC}}\sum_{k=1}^{\mathrm{MC}}[C_k(\mathbf{x},t)-\langle C(\mathbf{x},t)\rangle]^2 \tag{4}$$

$\sigma_C^2(\mathbf{x},t)$ represents the uncertainty in the predictions.

Fig. 4 shows the effect of the number of Monte-Carlo realizations on the stability of the ensemble and the standard deviation of the peak concentration. Fig. 4 leads to the conclusion that increasing the number of Monte-Carlo realizations from 50 to 100 realizations, in this particular problem, does not significantly affect the accuracy of the ensemble concentration and its standard deviation. The reason behind this is that conditioning on boreholes controls the geological structures so that they do not vary that much from one realization to another and leads to fast converges of the ensemble statistics. This is of course different from other Monte-Carlo methods that use stationary Gaussian random fields which need many realizations to converge (see Guadagnini and Neuman, 1999).

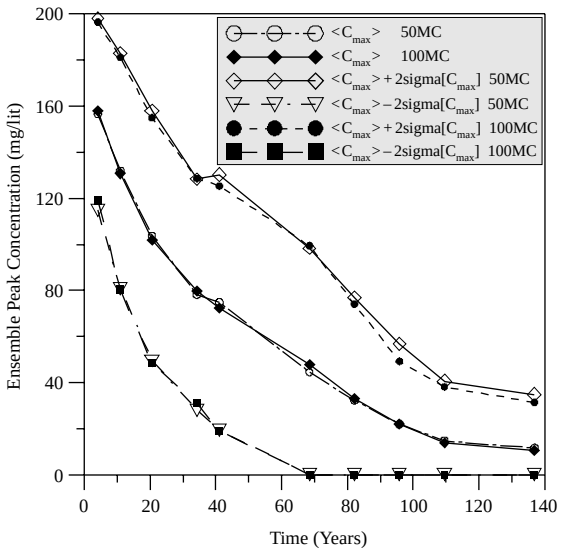

Fig. 4. Sensitivity analysis on the number of Monte-Carlo realizations.

A set of numerical experiments is performed according the conditioning scenarios given in Table 4. The conditioning is performed on sample data from the reference cross-section that is generated based on real data from the central Rhine-Meuse delta in the Netherlands. Single realizations of plume concentration, spatial moments and breakthrough curves are obtained and ensemble plume concentration and standard deviation plume concentration are computed for various conditioning scenarios at different times.

Table 4
Different conditioning scenarios considered in the study

Conditioning scenario #	No. of boreholes	Distance between boreholes (m)
1	2	240
2	3	120
3	5	60
4	9	30
5	13	20
6	17	15
7	25	10

5. Discussion of flow and transport simulation results

5.1. Single realizations analysis

5.1.1. Concentration fields

Plume snapshots at 41.1 and 82.2 years since release, and conditioned on 2, 3, 5, 9, 13, 17 and 25 boreholes are displayed in Fig. 5. It is important to mention that the actual drilling density in this section was 13 drillings at an equidistance of 20 m (Weerts and Bierkens, 1993). The high nugget value in their variograms suggests that the lithological variation in the section is actually larger than that is suggested by the 'ground truth'. We have investigated here many imaginary boreholes to study the convergence of the

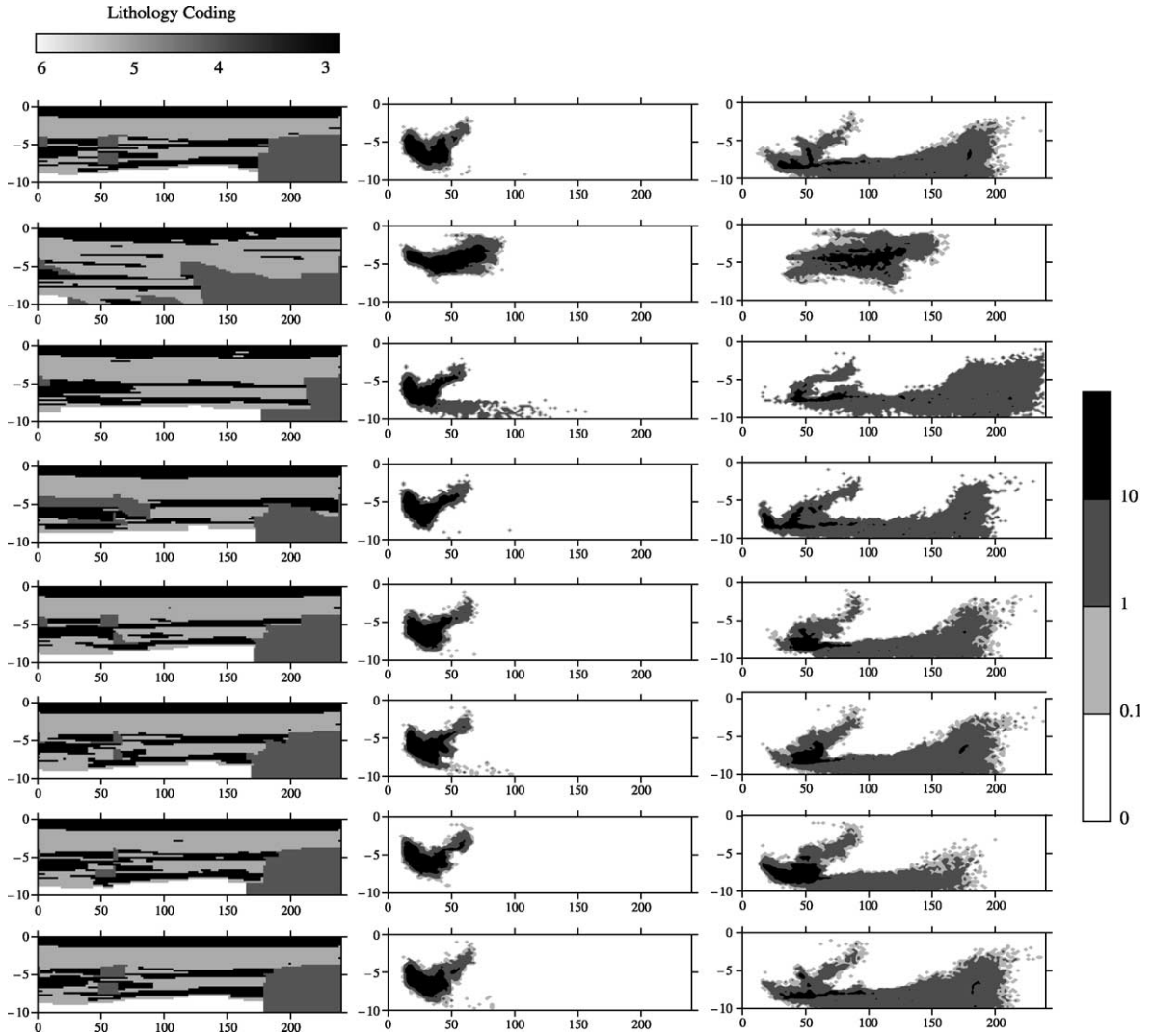

Fig. 5. Performance of conditioning with increasing the number of boreholes (from top to bottom: 2, 3, 5, 9, 13, 17 and 25 boreholes are used, respectively). Top image (left column) is the schematized original cross-section and all the next rows show the corresponding stochastic simulations of the geological structures (single realizations). Single realizations of the concentration distribution at $t=41.1$ years conditioned on the given boreholes (middle column). Single realizations of the concentration distribution at $t=82.2$ years conditioned on the given boreholes (right column), (concentration is in mg/l).

concentrations and plume statistics to concentration and plume statistics of the original section. Fig. 5 shows the enhancement of the shape of the concentration plume and the values of the concentration distribution with increasing number of conditioning boreholes. Conditioning on two boreholes is the worst case scenario. There is a pronounced improvement in the plume shape when conditioning is performed on three boreholes. Conditioning on five boreholes shows improvement in the plume front, which was lost when conditioning is performed on three boreholes. Increasing the number of boreholes from five onwards does not show significant improvement in the plume shape, however, the magnitude of the concentration seems to improve a lot. This is noticeable at the black zones with concentration larger than 10 mg/l (see Fig. 5 middle and right columns).

5.1.2. Peak concentration

Models are often used to predict peak concentrations. It is of practical interest to compare the maximum actual concentration at a given time (from the original section) with the maximum concentration computed from single realizations conditioned on number of boreholes. Fig. 6 displays the performance of the peak concentration at four different times (34.2, 68.4, 95.8 and 136.9 years) as a function of the number of conditioning boreholes. The curves show general trend towards the convergence of the peak concentration of the original section. The convergence is of oscillatory type this is due to the fact that some layers will become connected in one of the conditioning scenarios which leads to preferential flow within high permeable connective layers and high concentration (convective dominant flow). Whereas, in another conditioning scenario the layers may be disconnected with low permeable zones which would lead to flow barriers and low concentration (dispersive dominant flow). It is important to notice that the location of the peak concentration may change from one location to another due to the conditioning scenario. Conditioning on 21 boreholes could be satisfactory from a practical point of view at all times.

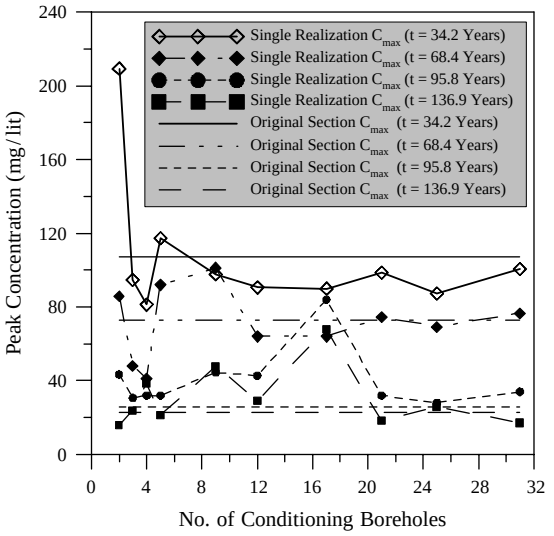

Fig. 6. Performance of conditioning on peak concentration (single realizations) at a number of snapshots $t = 34.2$, 68.4, 95.8, and 136.9 years, respectively.

5.1.3. Plume spatial moments

Fig. 7 shows single realizations of plume spatial moments (first and second moments) in the x- and y-directions, respectively. The simulations show that conditioning on three boreholes is the minimum requirement to produce the same trend as observed in the original section. However, conditioning on 5 up to 25 boreholes shows enhancement of the convergence towards the original section in terms of the magnitudes of the spatial moments.

5.1.4. Breakthrough curve

Fig. 8 shows the performance of the breakthrough curves due to conditioning on 2, 3, 5, 9 and 25 boreholes, respectively. It is important to mention that, the breakthrough curves are calculated for the normalized mass of the concentration in the modeled cross-section. The curves show enhancement due to conditioning.

5.1.5. Effect of borehole locations

A series of experiments has been performed to study the effect of an intermediate borehole location on the conditioning performance. In these experiments, we fixed the left boundary and right boundary boreholes. However, a single middle borehole was located at various locations at 30, 60, 90, 120, 150, 180, 210 m from the left boundary, respectively. The corresponding conditional geological simulation on these boreholes is shown in Fig. 9 (left column).

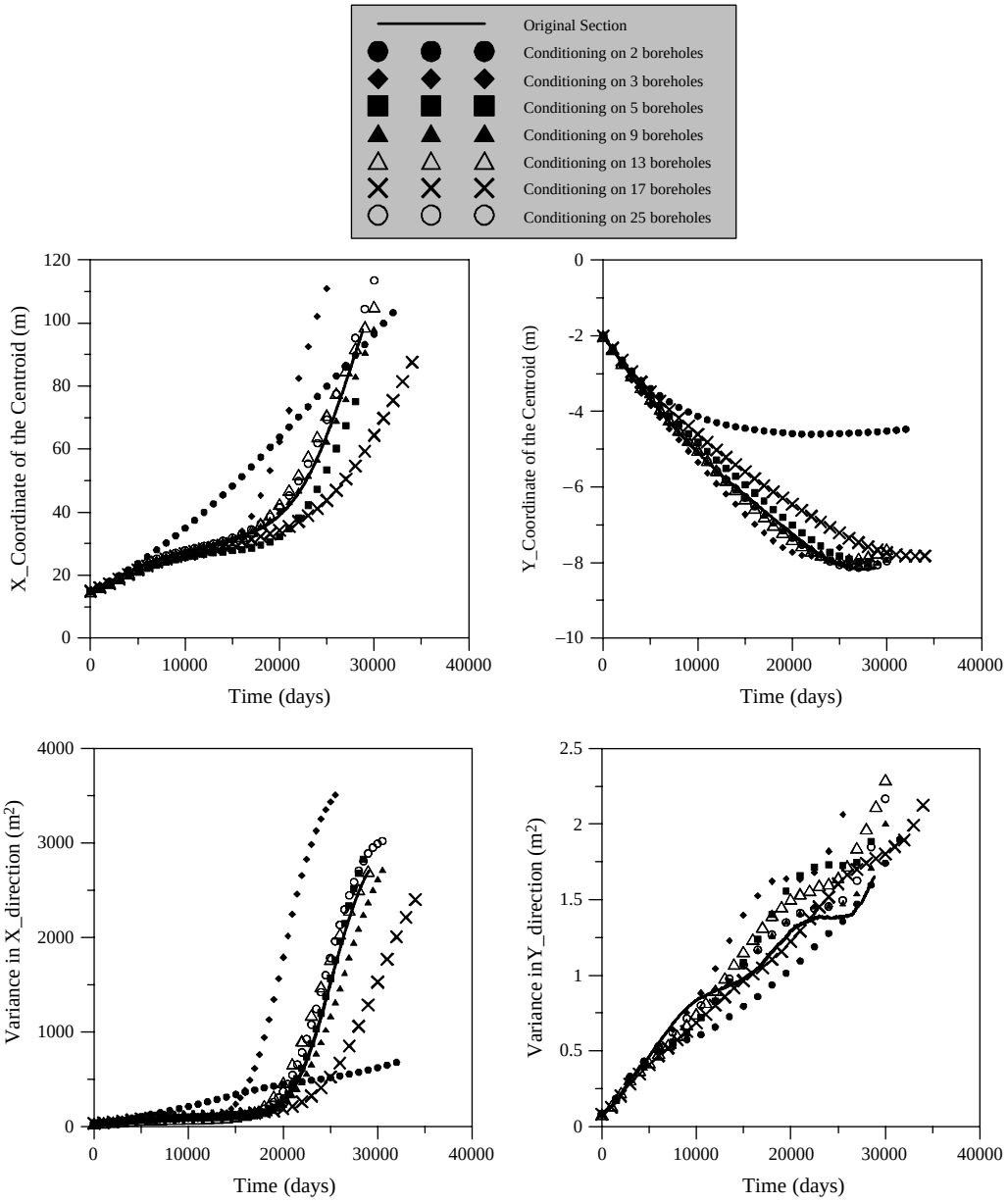

Fig. 7. Performance of conditioning on first and second plume spatial moments in *x*- and *y*-directions, respectively, of single realizations of the 240 m × 10 m cross-section shown in Fig. 1 when conditioned on 2, 3, 5, 9, 13, 17 and 25 boreholes, respectively, (top left image is the evolution of the *X*-coordinate of the centroid, top right image is the evolution of the *Y*-coordinate of the centroid, bottom left image is the evolution of the variance in *X*-coordinate and bottom right image is the evolution of the variance in *Y*-coordinate.

The flow and transport models are run on these geological realizations and displayed on the middle and right columns of Fig. 9 after 41.1 and 82.2 years since release. The simulations show the importance of a borehole location on capturing the actual shape of the plume. In the near field about 41.1 years since release, the best plume shape is obtained when the borehole is located at 30 m. However, in the far field

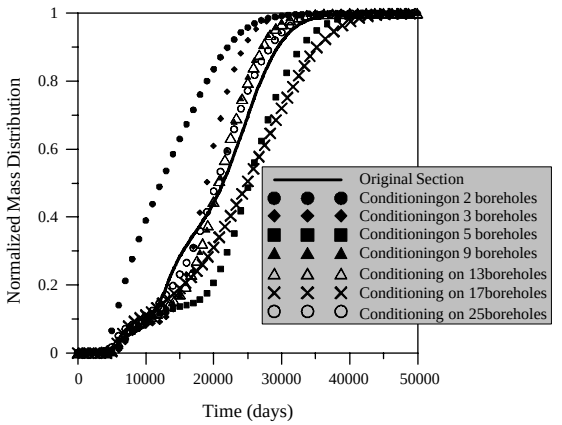

Fig. 8. Performance of conditioning on breakthrough curves at 40 m from the left side of the domain of single realizations of the 240 m × 10 m cross-section shown in Fig. 1 when conditioned on 2, 3, 5, 9, 13, 17 and 25 boreholes, respectively.

i.e. about 82.2 years since release, the best plume shape is obtained when conditioning is performed on a borehole located at 120 m. This leads to the conclusion that conditioning is dependent on the size of the plume. At early times, when the plume is small, conditioning on a 30 m borehole was sufficient to capture the significant heterogeneity that is in the order of magnitude of the plume size. It produces a plausible plume shape. In late times, the plume spreads on a larger area and the 30 m borehole is not anymore significant. However, the 120 m borehole captured the larger scale variability of the deposit leading to better representation of the plume.

5.2. Analysis of ensemble computational results

5.2.1. Ensemble concentration fields and standard deviations

Figs. 10–12 and 13 show a comparison between the evolution of actual plumes (simulated in the original cross-section) and ensemble plumes at some snapshots recorded at time $t=4.1$, 82.2, and 136.9 years, respectively. The reduction of uncertainty due to conditioning is computed as the difference between conditioning on a number of boreholes to conditioning on two boreholes only (minimum conditioning scenario). This difference is plotted for conditioning on 5 (Fig. 11), 9 (Fig. 12) and 25 (Fig. 13) boreholes, respectively. However, for conditioning on two boreholes the standard deviation in concentration fields are plotted as a reference. It is noticeable that the ensemble plumes are smoother in appearance in comparison with the corresponding actual plumes. This is due to the averaging procedure over the number of Monte-Carlo realizations. Conditioning enhances the prediction of the concentration distribution. It is clear from the figures that ensemble plumes converge to the actual plume shape by increasing the number of conditioning boreholes up to 25 boreholes. The ensemble average and ensemble standard deviation plumes (middle and right columns in Fig. 10) possess the same shape and they are covering a large area with respect to the actual plumes. Figs. 11–13 shows the reduced uncertainty due to conditioning. At early time there is almost no improvement, however, at large times the reduction in uncertainty is remarkable. The negative values mean reduction in the uncertainty, zero values mean no reduction in uncertainty and positive values means places with high uncertainty. It is noticeable that the highest plume uncertainty (black zones) is located in the plume fronts in the direction of the flow field and it is reduced once the front is getting diffused.

5.2.2. Ensemble peak concentration and coefficient of variation

Fig. 14 (left) shows the ensemble average peak concentration as a function of the conditioning boreholes at four snapshots. The graphs show the convergence of the ensemble average peak concentration towards the actual concentration (in the original section). It is obvious from the graph that even with 31 conditioning boreholes, the ensemble peak concentration is below the actual concentration in the original section. This has to do with averaging over the realizations that always lead to smoother concentration than in the actual section (see single realizations in Fig. 6).

Fig. 14 (right) shows the coefficient of variation of maximum concentration CV(C_{max}) at some snapshots as a function of the conditioning boreholes. The CV is relatively large (CV > 1) when conditioning is performed on two, three and four boreholes. This reflects high uncertainty in the peak concentration. However, a big reduction in the CV has been achieved by conditioning on five boreholes onwards. It is also clear from the figure that CV(C_{max}) increases in time

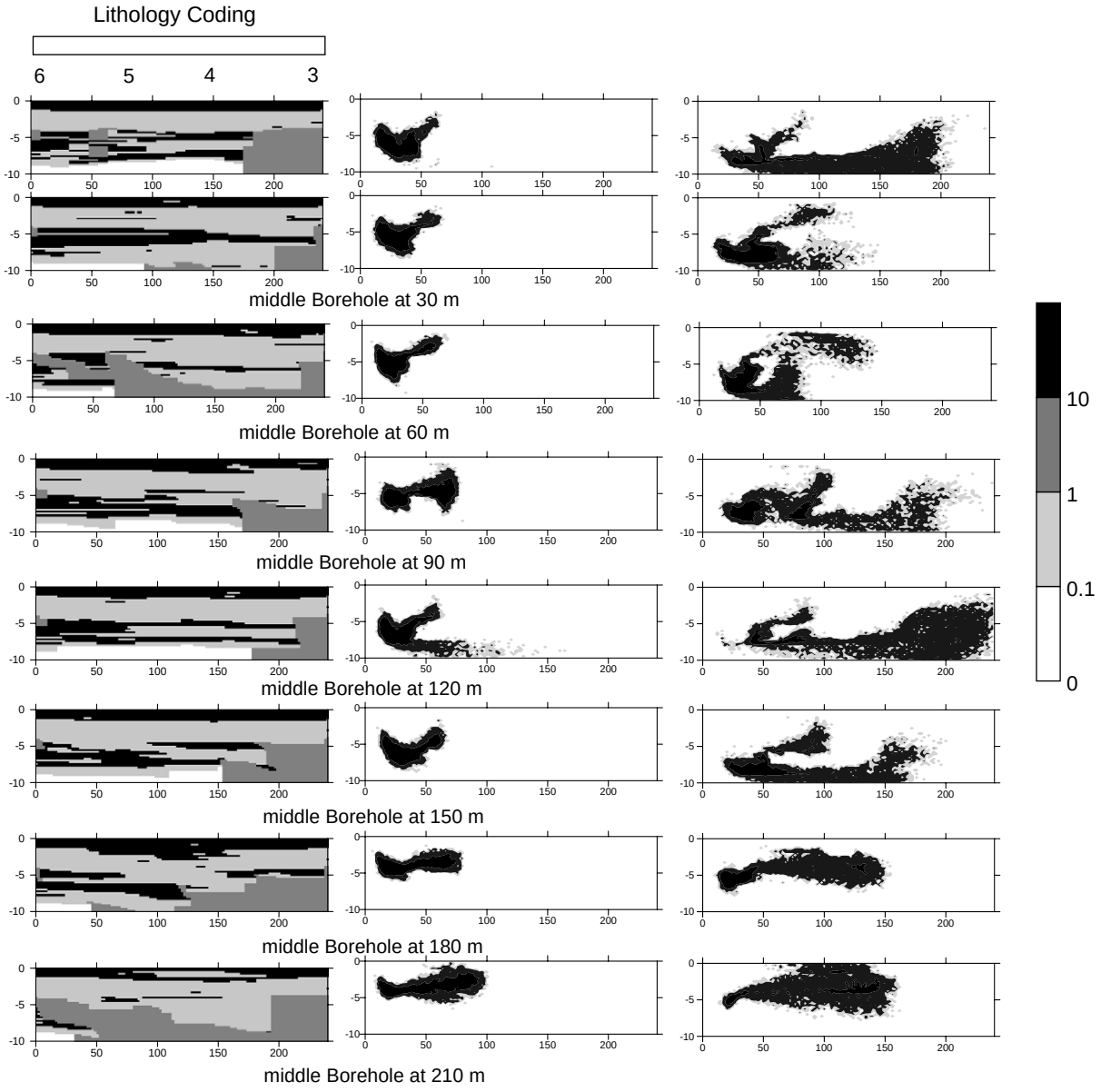

Fig. 9. Effect of borehole location. Performance of conditioning on three boreholes; two at the boundaries and a middle borehole at 30, 60, 90, 120, 150, 180, 210 m, respectively. Top most image (left column) is the schematized original cross-section and all the next rows show the corresponding stochastic simulations of the geological structures (single realizations). Single realizations of the concentration distribution at $t=$ 41.1 years conditioned on the given boreholes (middle column). Single realizations of the concentration distribution at $t=82.2$ years conditioned on the given boreholes (right column), (concentration is in mg/l).

after conditioning on 12 boreholes onwards and it does not significantly change when number of boreholes increases. The increase of CV($C_{\max}$) in time is due to the fact that the source is located in a low permeable zone which does not change over the realization due to conditioning and the flow is perpendicular to the layers (in the near field). This leads to plumes which do not change much in their

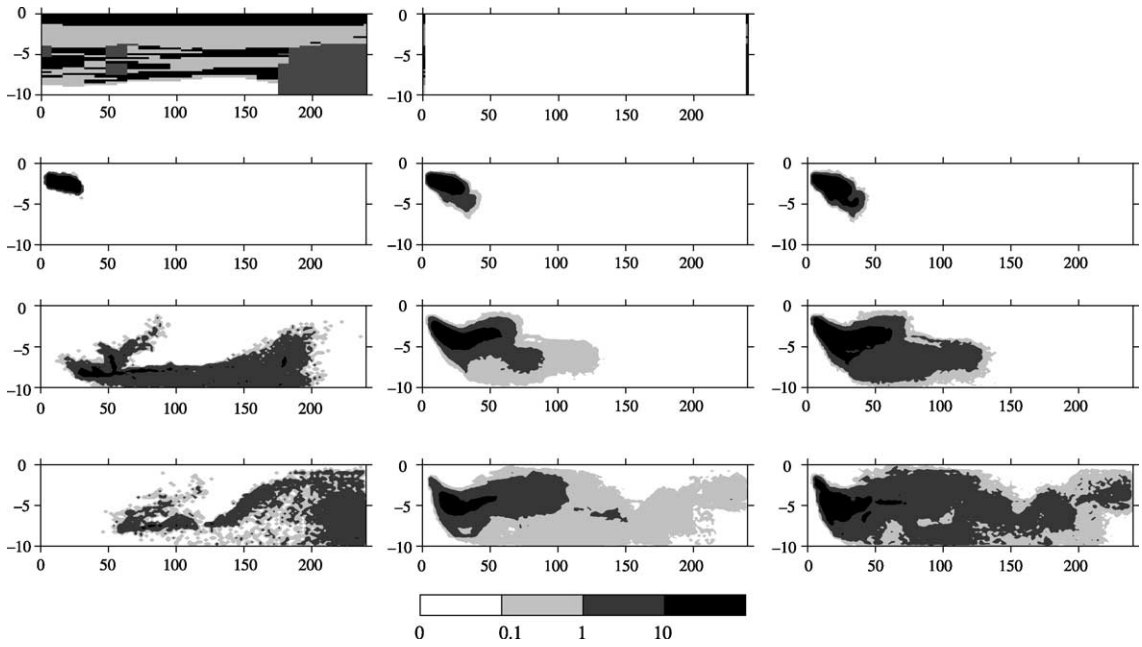

Fig. 10. Performance of conditioning on two boreholes: Top left is the 'real' cross-section. Next rows left column show the concentration fields of the actual cross-section at $t=4.1$, 82.2, and 136.9 years and from top to bottom). Middle column top image is the conditioning boreholes. Next rows middle column is the ensemble concentration field at the same times. Right column shows the ensemble standard deviation concentration fields at the same times.

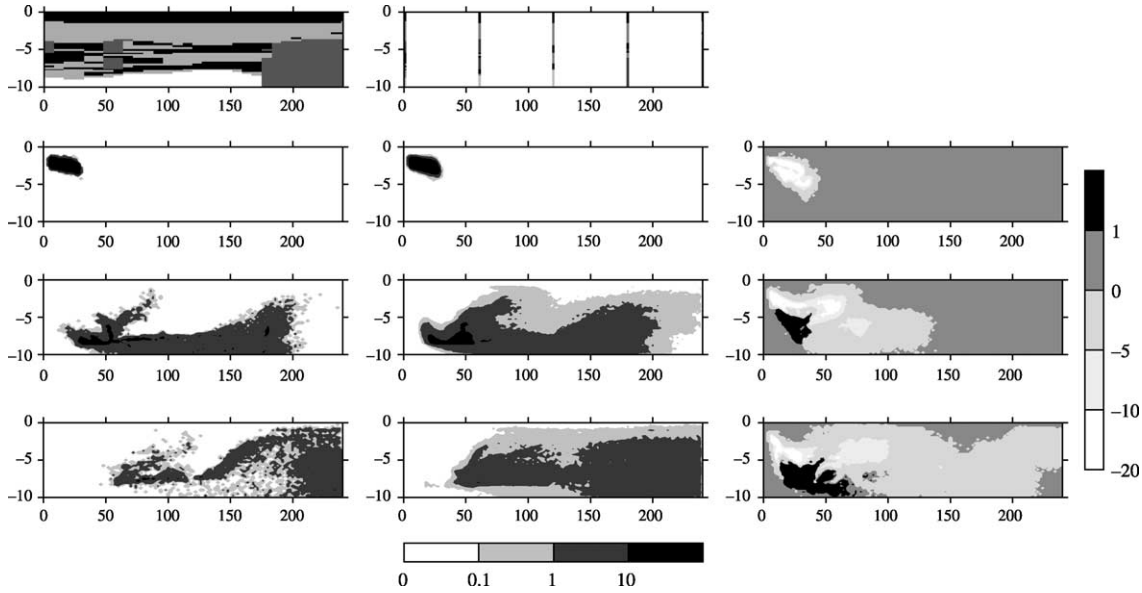

Fig. 11. Performance of conditioning on five boreholes: Top left is the 'real' cross-section. Next rows left column shows the concentration fields of the actual cross-section at $t=4.1$, 82.2, and 136.9 years and from top to bottom). Middle column top image shows the conditioning boreholes. Next rows middle column is the ensemble concentration field at the same times. Right column is the difference between ensemble standard deviation concentration fields conditioned on 25 boreholes and ensemble standard deviation concentration fields conditioned on two boreholes at the same times.

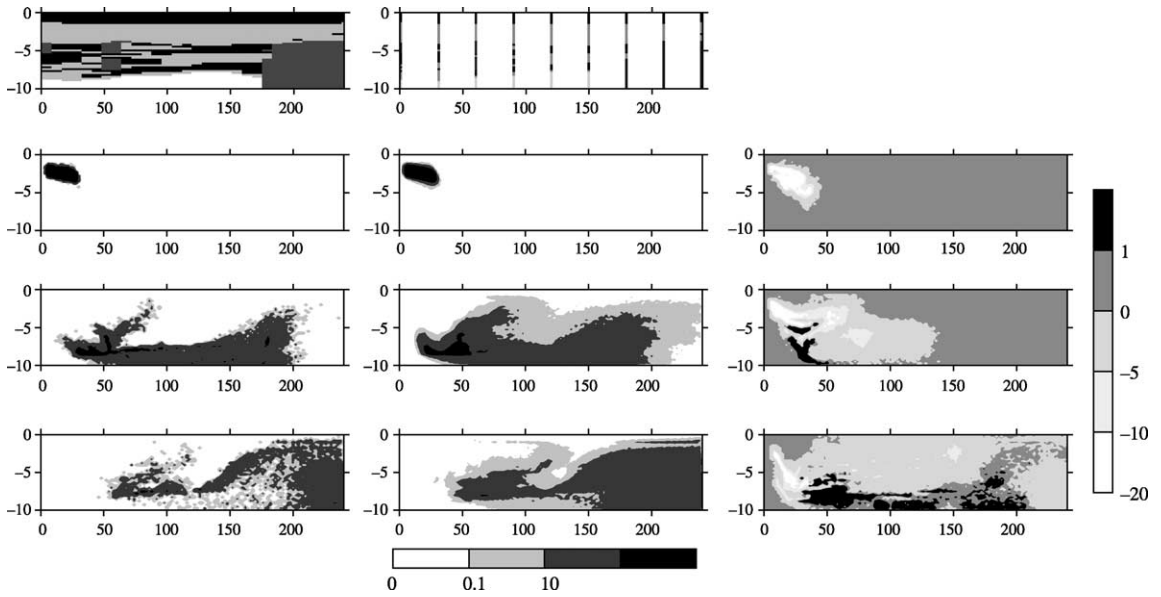

Fig. 12. Performance of conditioning on nine boreholes: Top left is the 'real' cross-section. Next rows left column is the concentration fields of the actual cross-section at $t=4.1$, 82.2, and 136.9 years and from top to bottom). Middle column top image is the conditioning boreholes. Next rows middle column is the ensemble concentration field at the same times. Right column is the difference between ensemble standard deviation concentration fields conditioned on nine boreholes and ensemble standard deviation concentration fields conditioned on two boreholes at the same times.

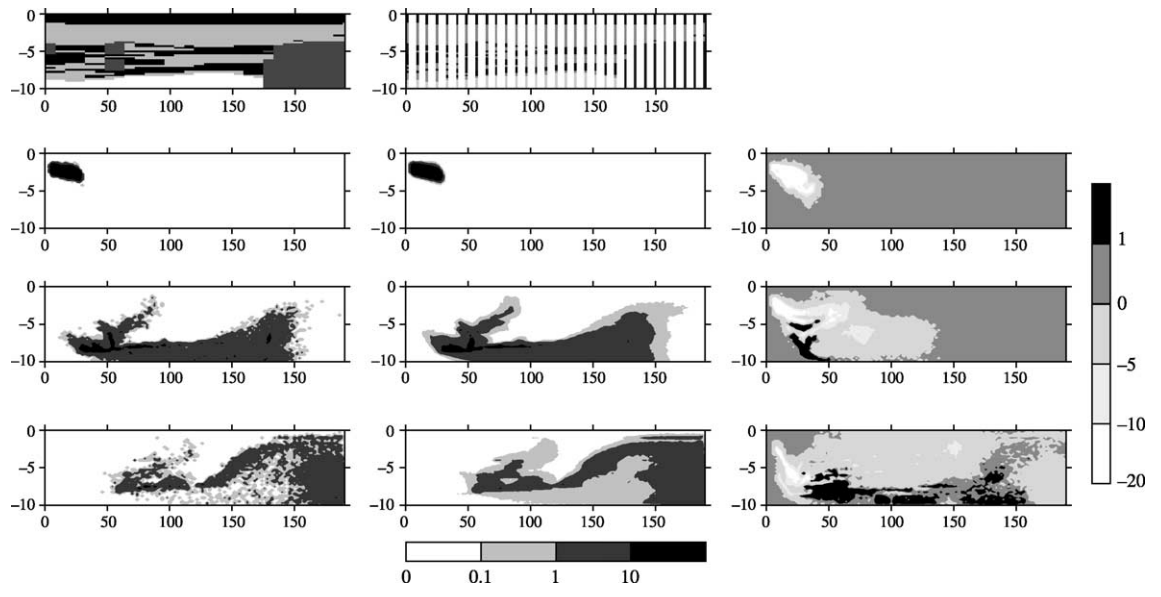

Fig. 13. Performance of conditioning on 25 boreholes: Top left is the 'real' cross-section. Next rows left column is the concentration fields of the actual cross-section at $t=4.1$, 82.2, and 136.9 years and from top to bottom). Middle column top image is the conditioning boreholes. Next rows middle column is the ensemble concentration fields at the same times. Right column is the difference between ensemble standard deviation concentration fields conditioned on 25 boreholes and ensemble standard deviation concentration fields conditioned on two boreholes at the same times.

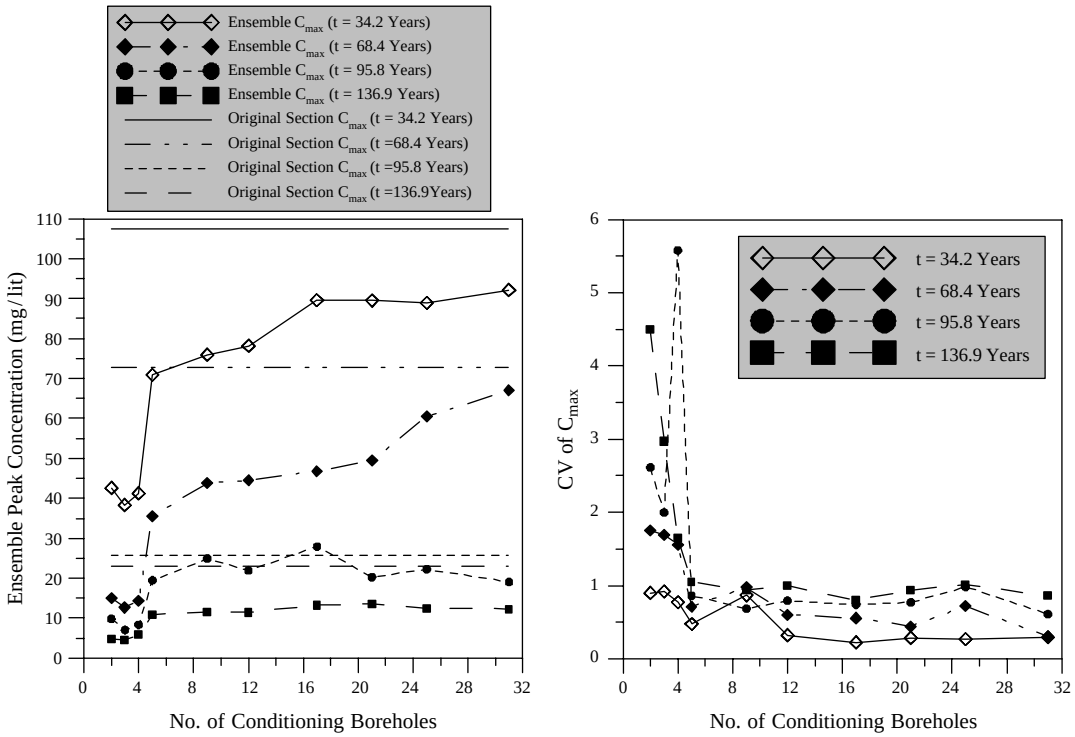

Fig. 14. Performance of conditioning on the ensemble peak concentration (left) and on the coefficient of variation of the ensemble peak concentration (right) at a number of snapshots $t = 34.2$, 68.4, 95.8, and 136.9 years, respectively. Conditioning is performed on 2, 3, 4, 5, 9, 12, 17, 21, 25 and 31 boreholes, respectively.

shapes over the realizations resulting in low coefficient of variation, however, when the plume gets far from the injection zone where the flow becomes nearly horizontal (i.e. in the far field) it spreads over larger area resulting in an increase of CV(C_{max}).

6. Conclusions

The following conclusions can be drawn,

1. The coupled Markov chain model proved to be a valuable tool in predicting the configuration of the heterogeneous geological structures which leads to reducing uncertainty in concentration distributions of contaminant plumes when reasonable amount of data is available.
2. In the current study, conditioning on 31 boreholes (spacing 8 m apart over a distance of 240 m) leads to the conclusion that a single realization plume is equivalent to its ensemble averaged plume. This means conditioning on a sufficient number of boreholes would lead to fulfilling ergodic conditions.
3. The ensemble concentration distribution and the ensemble standard deviation distribution have the same pattern. The ensemble concentration standard deviation is peaked at the location of the peak ensemble concentration and decreases when one goes far from the peak concentration. This result supports early work by Rubin (1991). However, in Rubin's case the maximum concentration was in the center of the plume which is attributed to Gaussian fields. The non-centered peak concentration, in this study, is attributed to the non-Gaussian multi-modal conductivity fields and the high contrast in hydraulic properties.
4. Reproduction of peak concentration, breakthrough curves, and the magnitude of plume spatial moments in a single realization require many conditioning boreholes (between 20 and 31

boreholes with 10–8 m spacing over a distance of 240 m in this case study, whereas the actual number of boreholes was 13). However, reproduction of plume shapes requires less boreholes (five suffice with 60 m spacing).

5. For single realization approach, convergence to the actual concentration is of oscillatory type. The reason behind this is that some layers are connected in one conditioning scenario which leads to preferential flows (advection dominant regime with high concentrations), while it may get disconnected in another conditioning scenario leading to flow barriers (dispersive dominant regime with low concentrations).

References

Bakr, M.I., te Stroet, C.B.M., Meijerink, A., 2003. Stochastic groundwater quality management: role of spatial variability and conditioning. Water Resour. Res. 39 (4), 1078–1092.

Bierkens, M.F.P., 1996. Modelling hydraulic conductivity of a complex confining layer at various spatial scales. Water Resour. Res. 32 (8), 2369–2382.

Bierkens, M.F.P., Weerts, H.J.T., 1994. Application of the indicator simulation to modeling the lithological properties of a complex confining layer. Geoderma 62 (15), 265–284.

Boggs, J.M., Young, S.C., Beard, L.M., Gelhar, L.W., Rehfeldt, K.R., Adams, E.E., 1992. Field study of dispersion in a heterogeneous aquifer, 1 Overview and site description. Water Resour. Res. 28 (12), 3281–3291.

Cross, G.R., Jain, A.K., 1983. Markov random field texture models. IEEE Trans. Pattern Anal. Mach. Int. 5 (1), 105–117.

Dagan, G., 1989. Flow and Transport in Porous Formations. Springer, New York.

Elfeki, A.M.M., Dekking, M., 2001. A Markov chain model for subsurface characterization: theory and applications. Math. Geol. 33 (5), 569–589.

Elfeki, A.M.M., Uffink, G.J.M., Barends, F.B.J., 1998. A coupled Markov chain model for quantification of uncertainty in transport in heterogeneous formations. In: Soares, A., Hernandez, J. (Eds.), GeoENV 98, Second European Conference on Geostatistics for Environmental Applications. Kluwer, Dordrecht.

Fischer, H.B., List, E.J., Koh, R.C.Y., Imberger, J., Brooks, N.H., 1979. Mixing in Inland and Coastal Waters. Academic Press, New York.

Galbraith, R.F., Walley, D., 1976. On a two-dimensional binary process. J. Appl. Probab. 13, 548–557.

Gelhar, L.W., 1993. Stochastic Subsurface Hydrology. Prentice Hall, Englewood Cliffs.

Guadagnini, A., Neuman, S.P., 1999. Nonlocal and localized analyses of conditional mean steady state flow in bounded, randomly nonuniform domains, 1, theory and computational approach. Water Resour. Res. 35 (10), 2999–3018.

Hess, K.M., Wolf, S.H., Celia, M.A., 1992. Large-scale natural gradient tracer test in sand and gravel, Cape Cod, Massachusetts, 3 Hydraulic conductivity and calculated macrodispersivities. Water Resour. Res. 28, 2011–2027.

Keshta. N.A.R., 2003. An application of stochastic models in groundwater pollution transport, MSc Thesis, Faculty of Engineering, Mansura University, Mansoura, Egypt, 145 p.

Lin, C., Harbaugh, J.W., 1984. Graphical Display of Two and Three-Dimensional Markov Computer Models in Geology. Van Nostrand Reinhold, New York.

Parks, K.P., Bentley, L.R., Crowe, A.S., 2000. Capturing geological realism in stochastic simulations of rock systems with Markov statistics and simulated annealing. J. Sediment. Res. 70 (4), 803–813.

Rubin, Y., 1991. Transport in heterogeneous porous media: prediction and uncertainty. Water Resour. Res. 27 (7), 1723–1738.

Smith, L., Schwartz, F.W., 1981. Mass transport. 2. Analysis of uncertainty in prediction. Water Resour. Res. 17 (2), 351–369.

Sudicky, E.A., 1986. A natural gradient experiment on solute transport in a sand aquifer: spatial variability of hydraulic conductivity and its role in the dispersion process. Water Resour. Res. 22 (13), 2069–2082.

Valstar, J.R., 2001. Inverse modeling of groundwater flow and transport, PhD Thesis, Delft University of Technology, Delft, The Netherlands, 229 p.

Van Beek, J.L., Koster, E.A., 1972. Fluvial and estuarine sediments exposed along the OUDE MAAS (The Netherlands). Sedimentology 19, 237–256.

Van Leeuwen, M., Butler, A.P., te Stroet, C.B.M., Tompkins, J.A., 2000. Stochastic determination of well capture zones conditioned on regular grid of transmissivity measurements. Water Resour. Res. 36 (4), 949–957.

Weber, K.J., Eijpe, R., Leijnse, D., Moens, C., 1972. Permeability distribution in Holocene distributary channel-fill near Leerdam (the Netherlands). Geologie en. Mijnbouw. 51, 53–62.

Weerts, H.J.T., 1996. Complex confining layers: architecture and hydraulic properties of holocene and late weichselian deposits in the fluvial rhine-meuse delta, The Netherlands, PhD Thesis, Utrecht university, The Netherlands, 189 p.

Weerts, H.J.T., Bierkens, M.F.P., 1993. Geostatistical analysis of overbank deposits of anastomosing and meandering fluvial systems; Rhine-Muese delta, the Netherlands. In: Fielding, C.R. (Ed.), Proceeding of the Fifth International Congress on Fluvial Sedimentology, Sedimentary Geology, vol. 85, pp. 221–232.